Nuclear Inst. and Methods in Physics Research B 458 (2019) 105–117

Contents lists available at ScienceDirect

Nuclear Inst. and Methods in Physics Research B

journal homepage: www.elsevier.com/locate/nimb

Measurement of activation cross sections of deuteron induced reactions on ^{nat}Ir in the 17–50 MeV energy range

F. Tárkányi[a], A. Hermanne[b], F. Ditrói[a,*], S. Takács[a], A.V. Ignatyuk[c]

[a] Institute for Nuclear Research, Hungarian Academy of Sciences (ATOMKI), Debrecen, Hungary
[b] Cyclotron Laboratory, Vrije Universiteit Brussel (VUB), Brussels, Belgium
[c] Institute of Physics and Power Engineering (IPPE), Obninsk 249020, Russia

ARTICLE INFO

Keywords:
Natural iridium target
Deuteron activation
Ir, Pt and Os radioisotopes
Cross section
Physical yield
Nuclear reaction model codes

ABSTRACT

In the frame of a thorough investigation of activation cross sections of deuteron induced nuclear reactions, excitation functions on iridium were investigated up to 50 MeV deuteron energy. Production cross sections were measured for the ^{193m}Pt, ^{191}Pt, ^{189}Pt, ^{188}Pt, ^{187}Pt, ^{194m2}Ir, ^{194g}Ir(m1 +), ^{192g}Ir(m1 +), ^{190m2}Ir, ^{190g}Ir(m1 +), ^{189}Ir, ^{188}Ir, ^{187}Ir and ^{191g}Os(m1 +) radionuclides. Activation method, stacked foil irradiation technique and off-line gamma-ray spectrometry were used for quantification of the radionuclides. The experimental results are compared with earlier data in the overlapping energy range. We discuss theoretical predictions obtained from the ALICE-IPPE-D and EMPIRE-II-D codes. The experimental data are also compared with calculated values reported in the TENDL-2017 on-line library calculated by using the TALYS code.

1. Introduction

In several previous studies we systematically investigated activation cross sections of deuteron induced reactions for accelerator technology, medical isotope production, labelling of industrial processes with radioactive tracers and for development of nuclear reaction theory [1] on a significant part of the Mendeljev's table (65 elements). We published data for the activation cross sections induced by deuterons on iridium (Ir) up to 40 MeV [2]. In the present study we extended the energy up to 50 MeV and re-measured the data in the 17–40 MeV energy range.

In the literature only two earlier experimental data sets were found: our earlier data reported in 2006 [2] and the recently published data of Obata et al. [3]. In our study [2] the experimental data were compared with the results of the ALICE-IPPE code [4], and Obata et al. compared their data with predictions in the TENDL-2015 library [5]. In the present study we extended the comparison with the results of the new version of ALICE-IPPE [4] and EMPIRE [6] D-versions, because they were modified for better description of deuteron induced reactions, and the latest version of TENDL-2017 [7].

2. Experiment and data evaluation

Elemental experimental cross sections were assessed by using the activation method, stacked foil irradiation technique and HPGe gamma-spectrometry. Cross-section data were calculated relative to the the ^{27}Al(d,x)^{22,24}Na monitor reactions [8], re-measured in the whole energy range.

The irradiation was made at one of the external beam lines of the Cyclone 90 cyclotron of the Université Catholique in Louvain la Neuve (LLN) for 60 min with a 50 MeV energy extracted beam having 100 nA beam intensity. The target package was irradiated in a short Faraday cup-like target holder. The irradiation, measurement and evaluation was similar to our previous work [9].

The irradiated stack contained 20 blocks of Ir (10.54 μm or 45.57 μm), Al (10 μm), Al (49.54 μm), Ta (19.29 μm), Al (49.54 μm). The 20 Ir targets covered the 50–17 MeV energy range. The target foils were high-purity metal foil, purchased from Goodfellow, the thickness of the sheets was individually checked by weight and area measurements. Five series of gamma-spectra were measured in the time intervals of 5.2–8.3 h, 21.5–32.3 h, 94.3–126.1 h and 774.9–1629.8 h, 3841.7–4377.1 h after the end of bombardment, respectively.

Our gamma spectra were evaluated by using the fitting algorithm of the Genie 2000 package or by an iterative method using the Forgamma [10,11] code in case of complex peaks.

For spectra evaluation, decay data from NUDAT-2.7 [12] and LUND/BNLL [13] were used (Table 1). So called elemental cross section were deduced considering the natural iridium target foils as being monoisotopic.

The Q values of the contributing nuclear reactions (Q value

* Corresponding author.
E-mail address: ditroi@atomki.hu (F. Ditrói).

https://doi.org/10.1016/j.nimb.2019.08.009
Received 29 April 2019; Received in revised form 13 August 2019; Accepted 13 August 2019
Available online 20 August 2019
0168-583X/

Table 1
Decay characteristics of the investigated reaction products and Q-values of reactions for their productions.

Nuclide (level) Decay mode	Half-life	E γ (keV)	I γ (%)	Contributing reaction	Q-value (keV)
^{193m}Pt	4.33 d	135.50	0.114547	^{193}Ir(d,2n)^{193}Pt	−3063.54
(149.783 keV)					
IT: 100%					
^{191}Pt	2.802 d	172.18	3.52	^{191}Ir(d,2n)^{191}Pt	−4017.43
ε: 100%		351.21	3.36	^{193}Ir(d,4n)^{191}Pt	−17987.54
		359.90	6.0		
		409.44	8.0		
		456.5	3.36		
		538.90	13.7		
^{189}Pt	10.87 h	141.18	3.6	^{191}Ir(d,4n)^{189}Pt	−19389.0
ε: 100%		243.50	5.9	^{193}Ir(d,6n)^{189}Pt	−33359.1
β^+: 0.44%		300.51	3.2		
		544.91	4.9		
		568.85	6.0		
		721.38	7.9		
^{188}Pt	10.2 d	187.59	19.4	^{191}Ir(d,5n)^{188}Pt	−26108.69
α: 2.6E-5%		195.05	18.6	^{193}Ir(d,7n)^{188}Pt	−40078.8
ε: 99.99997%		381.43	7.5		
		423.34	4.4		
^{187}Pt	2.35 h	106.46	9	^{191}Ir(d,6n)^{187}Pt	−35315.9
ε: 100%		110.04	5.7	^{193}Ir(d,8n)^{187}Pt	−49286.0
		304.71	4.3		
		709.17	5.2		
		819.21	3.7		
^{194m2}Ir	171d	338,8	55	^{193}Ir(d,p) ^{194}Ir	3842.224
(370 keV)		482,83	97		
β^-: 100%		562,6	70		
		687,7	59		
^{194g}Ir	19.28 h	293.541	2.5	^{193}Ir(d,p) ^{194}Ir	3842.224
β^-: 100%		328.448	13.1		
		645.146	1.18		
^{192}Ir	73.829 d	295.95650	28.71	^{191}Ir(d,p) ^{192}Ir	3973.554
ε: 4.76%		308.45507	29.70	^{193}Ir(d,p2n)^{192}Ir	−9996.55
β^-: 95.24 4%		316.50618	82.86		
		468.06885	47.84		
		604.41105	8.216		
		612.46215	5.34		
^{190m2}Ir	3.087 h	186.7	64.2	^{191}Ir(d,p2n)^{190}Ir	3973.554
(376.4 keV)		361.2	86.72	^{193}Ir(d,p4n)^{190}Ir	−9996.55
IT: 8.6%		502.5	89.38		
ε: 91.4 2%		616.5	90.14		
^{190g}Ir	11.78 d	186.68	52	^{191}Ir(d,p2n)^{190}Ir	−10251.1
ε: 100%		361.09	13.0	^{193}Ir(d,p4n)^{190}Ir	−24221.21
		371.24	22.8		
		407.22	23.9		
		518.55	34.0		
		557.95	30.1		
		569.30	28.5		
		605.14	39.9		
^{189}Ir	13.2 d	245.1	6.0	^{191}Ir(d,p3n)^{189}Ir	−16626.4
ε: 100%				^{193}Ir(d,p5n)^{189}Ir	−30596.5
				^{189}Pt decay	−19389.0
^{188}Ir	41.5 h	155.05	30	^{191}Ir(d,p4n)^{188}Ir	−24802.37
ε: 100%		477.99	14.7	^{193}Ir(d,p6n)^{188}Ir	−38772.48
β^+: 0.35%		633.02	18		
^{187}Ir	10.5 h	177.68	2.20	^{191}Ir(d,p5n)^{187}Ir	−31669.2
ε: 100%		427.02	3.7	^{193}Ir(d,p7n)^{187}Ir	−45639.3
β^+:0.0349%		610.88	3.5	^{187}Pt decay	−35315.9
		912.86	4.3		
		977.54	2.8		
		987.35	2.5		
^{191}Os	15.4 d	129.431	26.50	^{191}Ir(d,2p)^{191}Os	−1755.79
β^-: 100%				^{193}Ir(d,2p2n)^{191}Os	−15725.9

Abundance of isotopes in natural Ir-%: ^{191}Ir-37.3, ^{193}Ir-62.7.
The Q-values shown in Table 1 refer to formation of the ground state. Decrease Q-values for isomeric states with level energy of the isomer.
Increase the Q-values if compound particles are emitted by: pn → d + 2.2 MeV, p2n → t + 8.5 MeV, 2pn → ^{3}He + 7.7 MeV, 2p2n → α + 28.3 MeV.

calculator [14]) are shown in Table 1 to show the reaction thresholds.

Uncertainties of the cross-sections were determined based on the recommendation in [15] by taking the sum in quadrature of all individual linear contributions: beam current (7%), target thickness or homogeneity (5%), detector efficiency (5%), photo peak area determination and counting statistics (1–20%).

Median beam energies in the target foils were obtained by using a degradation calculation based on the calculated primary energy, the stopping powers data of Anderson and Ziegler [16] and the fitted monitor reactions (Fig. 1) [17]. A correction of the beam monitor

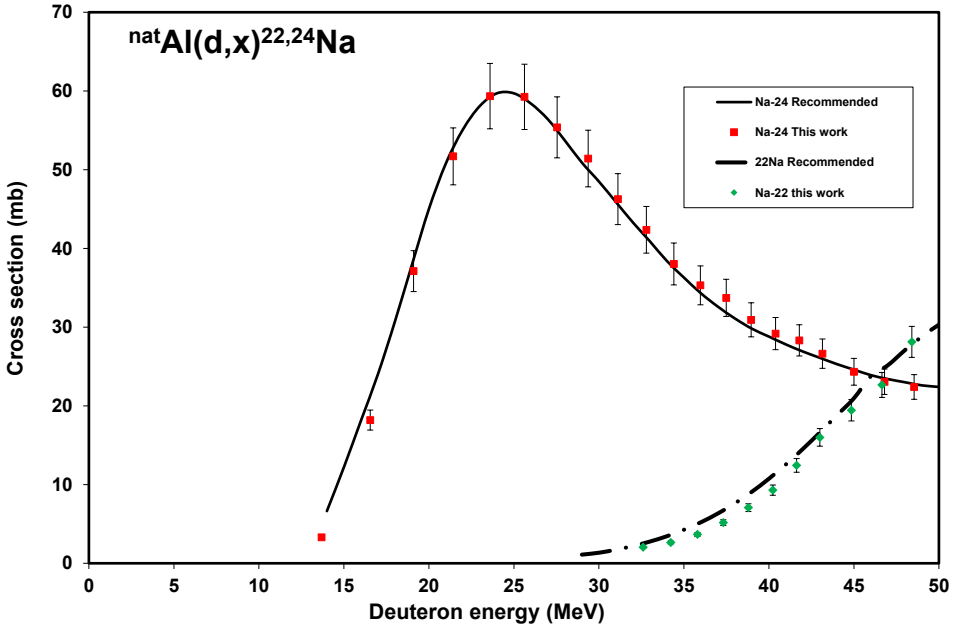

Fig. 1. Cross sections of the reactions on Al monitor foils compared with the recommended values.

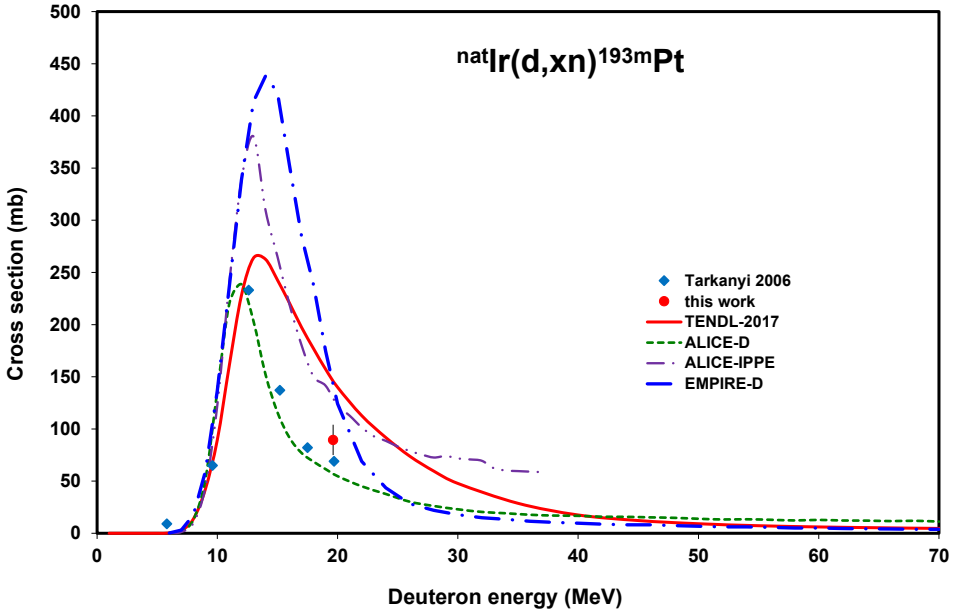

Fig. 2. Excitation function of the $^{nat}Ir(d,xn)^{193m}Pt$ reaction.

values based on the monitor reactions was not necessary. Uncertainties of the energy points were estimated by taking into account cumulative effects during the particle path through the matter (primary energy, target thickness, energy straggling) and the necessary correction from monitor reaction. The primary energy uncertainty was received from the energy calibration of the particular accelerator, the energy uncertainties during the beam passing through the stack was estimated by using Monte-Carlo penetration code [18].

3. Theoretical calculations

The cross sections of the investigated reactions were calculated using the pre-compound model codes ALICE-IPPE [4] and EMPIRE-II [6], modified for deuterons by Ignatyuk (D versions) [19]. These modified codes, in which a simulation of direct (d, p) and (d, t) transitions with the general relations for a nucleon transfer probability in the continuum is included through an energy dependent enhancement factor for the corresponding transitions, are named ALICE-D and EMPIRE-D. The theoretical curves were determined using one recommended input data-set [20] without any optimization or adjustment of parameters to the individual reactions or stable target isotopes. Independent data for isomers with ALICE-D code was obtained by using the isomeric ratios calculated with EMPIRE-D. We also reproduce in the figures predictions of ALICE-IPPE reported by us in [2], and for some reactions, predictions from systematics of nuclear reactions in the same mass region.

The experimental data are also compared with the cross section data reported in the TENDL-2017 [7] on-line nuclear reaction data library. The TENDL library was developed on the basis of the TALYS nuclear model code system [21] for direct use in both fundamental physics and applications (default TALYS calculations).

Table 2
Experimental cross sections for the ^{nat}Ir(d,xn)^{193m,191,189,188,187}Pt reactions.

Energy		^{193m}Pt		^{191}Pt		^{189}Pt		^{188}Pt		^{187}Pt	
E	△E	σ	△σ	σ	△σ	σ	△σ	σ	△σ	σ	△σ
MeV		mb									
49.50	0.20			131.78	15.75	500.31	59.74	249.61	29.80	67.45	8.28
47.86	0.28			145.94	17.44	450.45	53.81	302.15	36.07	52.21	6.40
46.18	0.31			153.16	18.29	356.04	42.55	377.10	45.05	27.52	3.47
44.45	0.34			170.57	20.37	277.94	33.24	319.09	38.07	13.61	1.85
42.93	0.38			217.85	26.03	273.32	32.69	403.43	48.62	6.33	0.88
41.62	0.41			240.97	28.78	268.37	32.10	337.79	40.31		
40.28	0.45			263.16	31.43	287.23	34.41	273.76	32.65		
38.90	0.50			308.99	36.88	328.12	39.15	223.73	26.73		
37.49	0.55			365.56	43.62	376.35	44.96	209.13	25.13		
36.03	0.60			419.48	50.05	415.48	49.65	158.58	19.14		
34.52	0.66			493.85	58.91	436.33	52.13	111.16	13.87		
32.96	0.73			536.09	63.95	409.55	48.97	39.28	4.86		
31.34	0.80			537.17	64.09	378.83	45.33				
29.65	0.88			488.95	58.33	310.50	37.13				
27.88	0.97			394.03	47.02	195.77	23.44				
26.02	1.07			257.76	30.78	84.21	10.26				
24.04	1.18			114.53	13.71	16.87	2.28				
21.92	1.29			71.27	8.56	13.26	1.92				
19.63	1.42	89.52	14.53	112.96	13.53						
17.09	1.57			170.78	20.42						

Table 3
Experimental cross sections for the ^{nat}Ir(d,x)^{194m2,194g,192,190m2,190g}Ir reactions.

Energy		^{194m2}Ir		^{194g}Ir		^{192}Ir		^{190m2}Ir		^{190g}Ir	
E	△E	σ	△σ	σ	△σ	σ	△σ	σ	△σ	σ	△σ
MeV		mb									
49.50	0.20	0.37	0.05	10.64	1.33	137.64	16.40	24.06	2.88	111.64	13.31
47.86	0.28	0.35	0.05	11.06	1.37	145.76	17.37	22.25	2.66	112.77	13.45
46.18	0.31	0.38	0.05	13.89	1.70	144.88	17.27	20.72	2.48	122.32	14.59
44.45	0.34	0.36	0.05	13.19	1.61	150.96	17.99	18.84	2.26	104.14	12.42
42.93	0.38	0.45	0.08	16.38	2.00	168.55	20.09	20.10	2.40	125.42	15.02
41.62	0.41	0.43	0.06	19.43	2.35	176.63	21.05	18.14	2.17	119.72	14.28
40.28	0.45	0.41	0.06	18.83	2.29	165.98	19.78	16.14	1.94	110.25	13.14
38.90	0.50	0.41	0.06	21.17	2.56	171.19	20.40	15.66	1.88	114.17	13.62
37.49	0.55	0.45	0.06	21.47	2.60	178.25	21.24	13.85	1.66	116.72	13.93
36.03	0.60	0.50	0.07	23.19	2.81	169.12	20.15	12.09	1.45	109.84	13.11
34.52	0.66	0.53	0.08	25.95	3.14	170.69	20.35	11.13	1.34	106.21	12.69
32.96	0.73	0.51	0.07	28.40	3.43	157.78	18.80	9.28	1.13	92.39	11.02
31.34	0.80	0.56	0.07	31.28	3.78	145.64	17.36	7.11	0.87	84.84	10.11
29.65	0.88	0.57	0.08	35.66	4.28	133.04	15.86	5.39	0.66	71.65	8.54
27.88	0.97	0.58	0.08	40.50	4.85	108.67	12.95	3.22	0.41	53.99	6.44
26.02	1.07	0.49	0.07	49.08	5.88	93.68	11.16	1.96	0.26	39.03	4.68
24.04	1.18	0.51	0.07	59.04	7.06	83.74	9.98	0.87	0.12	27.64	3.30
21.92	1.29	0.54	0.07	69.21	8.27	76.74	9.15	0.49	0.08	16.69	1.99
19.63	1.42	0.43	0.06	83.70	10.00	79.16	9.43	0.34	0.06	10.92	1.30
17.09	1.57	0.44	0.06	109.17	13.03	91.85	10.95	0.48	0.08	13.77	1.65

4. Results and discussion

4.1. Cross sections

Cross sections of the nuclear reactions ^{nat}Ir(d,xn)^{193m}Pt,^{191}Pt,^{189}Pt,^{188}Pt,^{187}Pt, ^{194m2}Ir,^{194g}Ir, ^{192}Ir,^{190m2}Ir,^{190g}Ir, ^{189}Ir,^{188}Ir,^{187}Ir,^{191}Os were determined experimentally and compared to the results of model calculation and are presented in Figs. 1–15. The numerical results for the cross sections are also presented in Tables 2–4. The different reaction product radio-isotopes are discussed separately below. Note, that in this work "cumulative" means cross sections, which includes, in addition to the direct formation of the referred nuclide, contributions of parent nuclides and/or isomeric states after their total decay. Cumulative cross sections are hence valid only after an appropriate cooling time. Moreover, note that in this work expressions like direct reaction, direct process, etc. do not refer to the reaction mechanism, but it means that there is no decay into the referred nuclide and it is used to emphasis that no cumulative process takes place.

4.1.1. ^{nat}Ir(d,xn)^{193m}Pt process

The product nucleus does not emit γ-rays during the decay of the ground state and decay of the metastable state is followed by a very low abundance and low-energy gamma-line (see Table 1). It was possible to measure this weak gamma-line and to calculate cross sections for ^{193m}Pt formation after subtracting the contribution from the similarly weak gamma-line of ^{192g}Ir (136.34 keV, 0.183%). Because the series of measurements was not particularly optimized for this radioisotope only one measured point had enough statistics to include. The results are shown in Fig. 2. The ^{193m}Pt could be formed by ^{191}Ir(d, γ) and ^{193}Ir (d,2n) reactions, however, only the latter will be taken into account as

Table 4
Experimental cross sections for the ^{nat}Ir(d,x)^{189,188,187}Ir,^{191}Os reactions.

Energy		^{189}Ir		^{188}Ir		^{187}Ir		^{191}Os	
E	△E	σ	△σ	σ	△σ	σ	△σ	σ	△σ
MeV		Mb							
49.50	0.20	274.94	32.79	21.30	2.68	140.43	16.93	2.42	0.29
47.86	0.28	272.43	32.68	15.75	2.01	102.01	12.38	3.64	0.48
46.18	0.31	266.51	31.80	19.12	2.38	60.36	7.42	1.10	0.18
44.45	0.34	257.89	30.75	16.75	2.09	20.75	2.80	0.00	0.00
42.93	0.38	296.78	35.40	14.84	1.87	9.82	1.58	2.38	0.44
41.62	0.41	346.64	41.36	11.71	1.57			2.81	0.37
40.28	0.45	366.21	43.69	8.84	1.28			2.38	0.30
38.90	0.50	391.35	46.72	6.98	1.13			0.64	0.28
37.49	0.55	369.85	44.11	4.95	1.00			0.00	0.00
36.03	0.60	339.54	40.47					1.11	0.21
34.52	0.66	271.30	32.34					0.47	0.44
32.96	0.73	162.89	19.44					1.48	0.20
31.34	0.80	59.52	7.22					0.00	0.00
29.65	0.88	6.90	0.94					1.16	0.16
27.88	0.97							1.12	0.17
26.02	1.07							1.85	0.28
24.04	1.18							1.82	0.23
21.92	1.29							1.83	0.23
19.63	1.42							1.16	0.14
17.09	1.57							1.22	0.15

it is known that (d, γ) reaction have extremely low cross-sections. The shapes of the theoretical curves follow the shape of experimental data, but there are significant disagreements regarding the magnitude of cross sections.

4.1.2. ^{nat}Ir(d, xn)^{191}Pt process

The first peak of the excitation function (Fig. 3) is due to the ^{191}Ir (d,2n) reaction and the second one is due to the ^{193}Ir(d,4n) reaction. The agreement with all earlier experimental data is acceptable. There are large differences in magnitude of cross sections between the predictions of the different model codes. The second maximum of theoretical predictions of ALICE-D and TENDL-2017 is shifted to lower energy.

4.1.3. ^{nat}Ir(d, xn)^{189}Pt process

There are large disagreements in value and energy of the maxima of excitation functions of ^{191}Pt between the measured experimental values and data calculated with different codes (Fig. 4). The new results are in acceptable agreement with the published previous experimental data.

4.1.4. ^{nat}Ir(d, xn)^{188}Pt process

In the studied energy range only the ^{191}Ir(d,5n) reaction has contribution to the production of ^{188}Pt. The agreement between the experimental data is good (Fig. 5), but the theoretical predictions differ significantly in energy dependence and cross section values.

4.1.5. ^{nat}Ir(d, xn)^{187}Pt process

In the measured energy range only the ^{191}Ir(d,6n) reaction contributes. The TENDL and ALICE-D predictions overestimate or the calculated excitation functions are shifted to low energy (Fig. 6). A considerable agreement is shown with EMPIRE-D predictions. No earlier experimental data were found in the literature.

4.1.6. ^{nat}Ir(d,xn)^{194m2}Ir and ^{nat}Ir(d,xn)^{194g}Ir(m1 +) processes

The radionuclide ^{194}Ir has three excited states. The first very short-lived metastable state ^{194m1}Ir (19.28 ms) decays by isomeric transition to the ^{194g}Ir ground-state (19.28 h), which itself decays with β$^-$ (100%) to stable ^{194}Pt. The second, higher laying, long half-life ^{194m2}Ir state (171 d) decays independently to stable ^{194}Pt. We could determine production cross sections for both ^{194m2}Ir and ^{194g}Ir. A good agreement with the earlier experimental data is noted. The ^{194g}Ir cross sections contain the direct production via ^{193}Ir(d,p) reaction and the contribution of the ^{194m1}Ir decay. The experimental and the theoretical excitation functions are shown in Figs. 7 and 8. No TENDL data are available for production of ^{194m2}Ir, and the ALICE-D and EMPIRE-D significantly overestimate the experimental data (Fig. 7). In case of ^{194g}Ir the TENDL significantly underestimates the experimental data, while for ALICE-D and EMPIRE-D the agreement is acceptable, as for the data from systematics (Fig. 8).

4.1.7. ^{nat}Ir(d, x)^{192g}Ir(m1 +) process

The measured cumulative cross sections consist of the cross sections of direct ^{192g}Ir (73.83 d) formation and total decay of short-lived metastable ^{192m1}Ir. The second metastable state (^{192m2}Ir) has very long

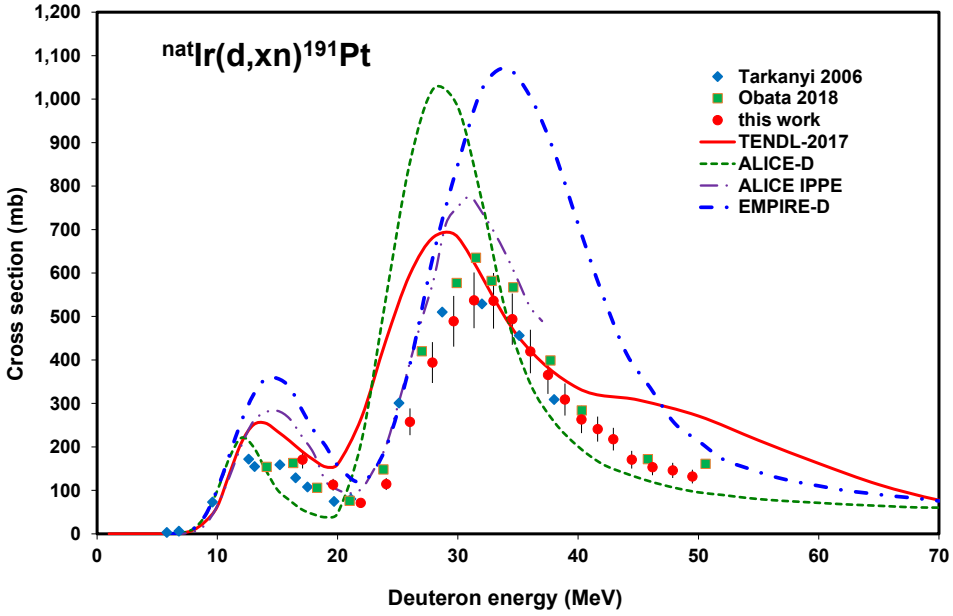

Fig. 3. Excitation function of the ^{nat}Ir(d,xn)^{191}Pt reaction.

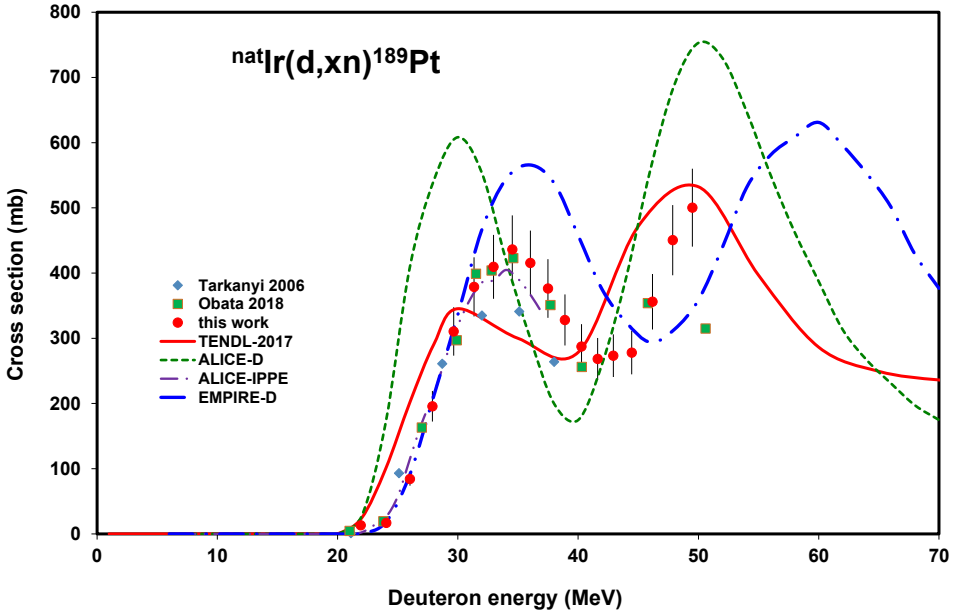

Fig. 4. Excitation function of the ^{nat}Ir(d,xn)^{189}Pt reaction.

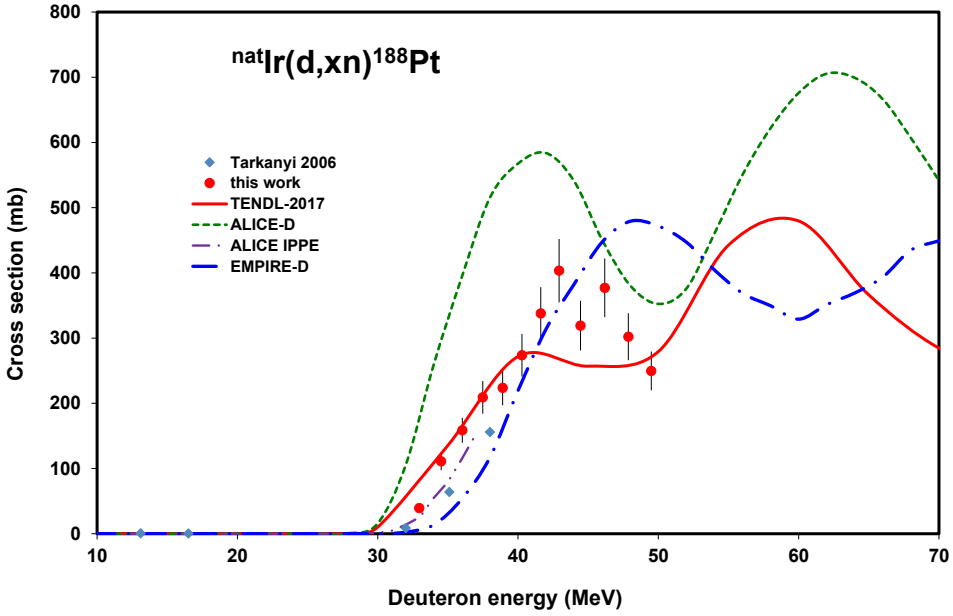

Fig. 5. Excitation function of the ^{nat}Ir(d,xn)^{188}Pt reaction.

half-life (241 years) and hence there is no practical contribution under the present experimental circumstances. The agreement with the earlier experimental data is acceptably good (Fig. 9). The contradiction between the measured and the theoretical predictions is significant and shows a fundamental difference between the TALYS results (TENDL-2017) and the other codes

4.1.8. ^{nat}Ir(d, pxn)^{190m2}Ir and ^{nat}Ir(d, pxn)^{190g}Ir(m1 +) processes

The results are shown in Fig. 10. The product nucleus has two high laying isomeric states (^{190m1}Ir (26.1 keV, 1.120 h, IT 100%) and ^{190m2}Ir (376.4 keV, 3.087 h) in addition to the ground state (11.78 d). We obtained cross section data for production of ^{190m2}Ir (Fig. 10) and for cumulative production of the ground state (Fig. 11). No earlier

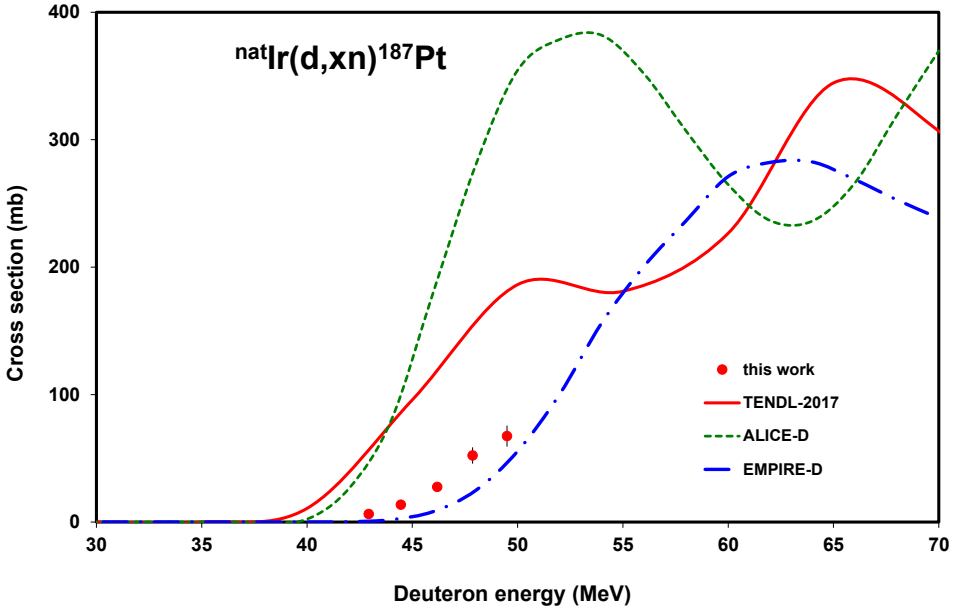

Fig. 6. Excitation function of the ^{nat}Ir(d,xn)^{187}Pt reaction.

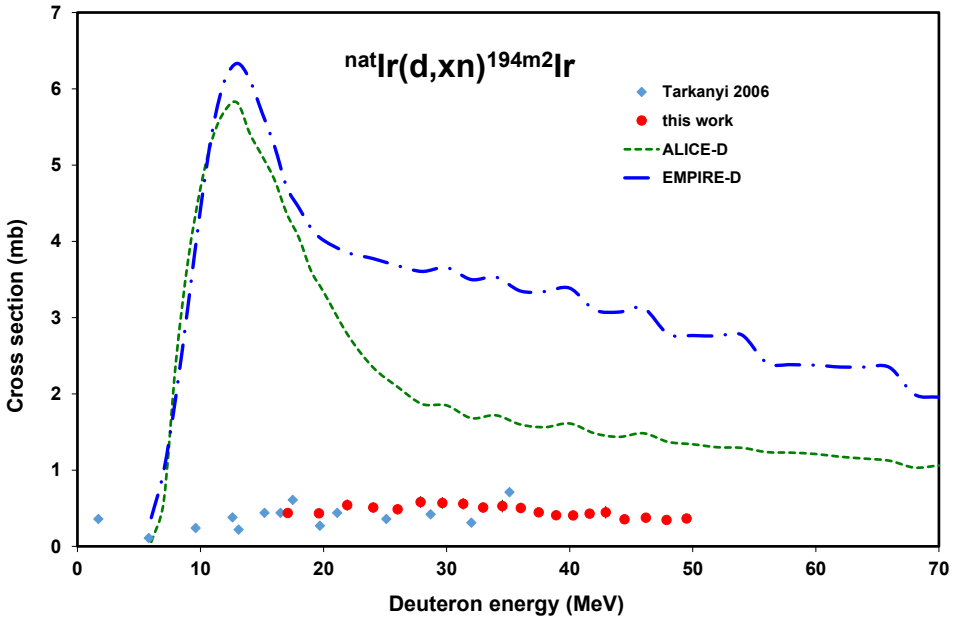

Fig. 7. Excitation function of the ^{nat}Ir(d,x)^{194m2}Ir reaction.

experimental data were found for ^{190m2}Ir production. The agreement between the measured results and the predictions calculated with the ALICE-D and EMPIRE-D codes is good, but in case of the TENDL model code (Fig. 10) the disagreement is significant.

In case of ^{190g}Ir the agreement of the experimental data is excellent. The predictivity of ALICE-D and EMPIRE-D is poor here, in opposition to a rather good TENDL (Fig. 11).

4.1.9. ^{nat}Ir(d, x)^{189}Ir process

The cumulative cross sections measured for the production of ^{189}Ir contain the contribution from ^{189}Pt (half-life: 10.87 h) after its complete decay. The comparison of the experimental and theoretical data shows large disagreement over the whole energy range (Fig. 12).

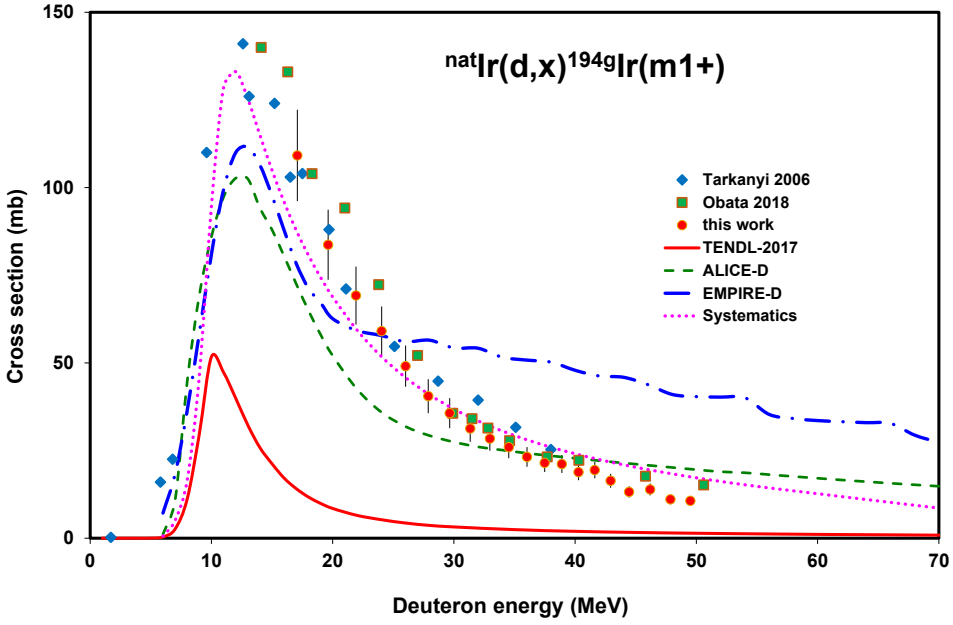

Fig. 8. Excitation function of the ^{nat}Ir(d,x)^{194g}Ir(m1 +) reaction.

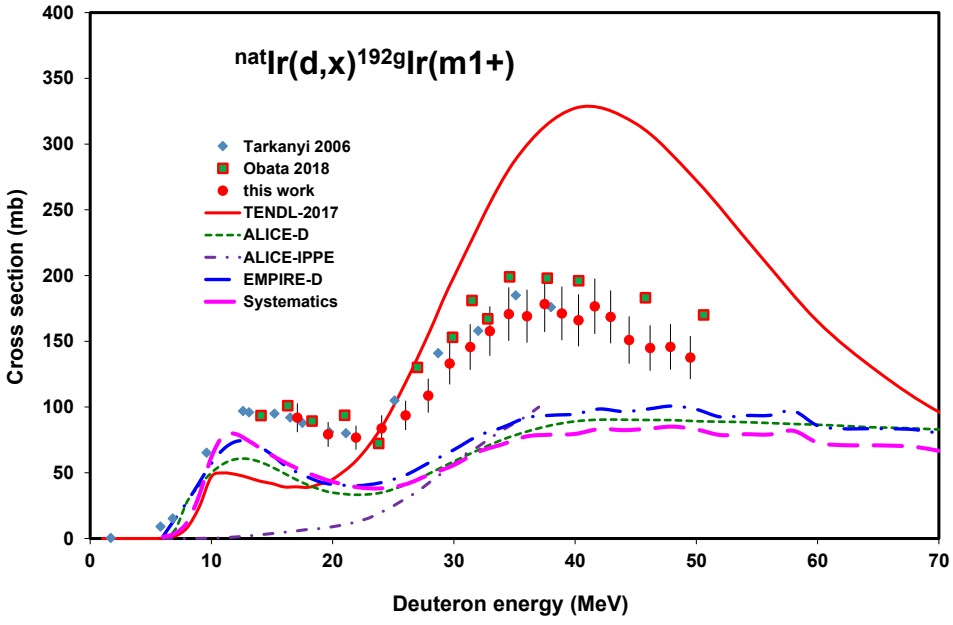

Fig. 9. Excitation function of the ^{nat}Ir(d,x)^{192g}Ir(m1 +) reaction.

4.1.10. ^{nat}Ir(d, x)^{188}Ir process

The cross section for the direct production of ^{188}Ir (41.5 h) was deduced from the first spectra measured after EOB by subtracting the contribution of the longer-lived ^{188}Pt (10.2 d) parent. The agreement with the TENDL-2017 is acceptable, the overestimation of the ALICE-D and EMPIRE-D codes is significant (Fig. 13). No earlier experimental data are available.

4.1.11. ^{nat}Ir(d, x)^{187}Ir process

The cross sections for ^{187}Ir (10.5 h) formation are cumulative, measured after complete decay of its shorter-lived ^{187}Pt parent (2.35 h). The results of the three theoretical codes differ significantly both in shape and in magnitude (Fig. 14). The prediction of TENDL-2017 is in acceptable agreement with our new experimental results. No earlier experimental data were found.

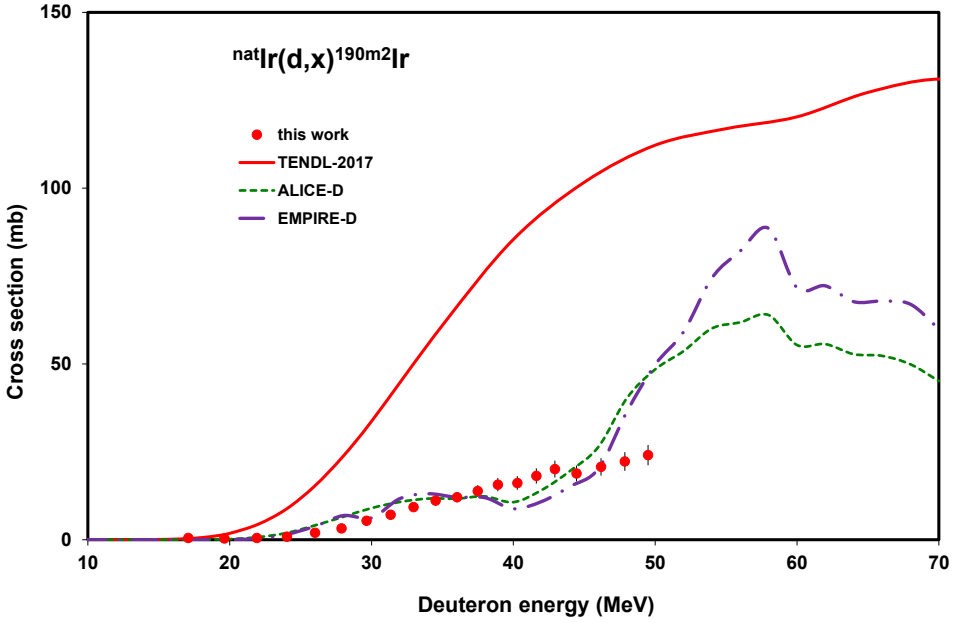

Fig. 10. Excitation function of the ^{nat}Ir(d,x)^{190m2}Ir reaction.

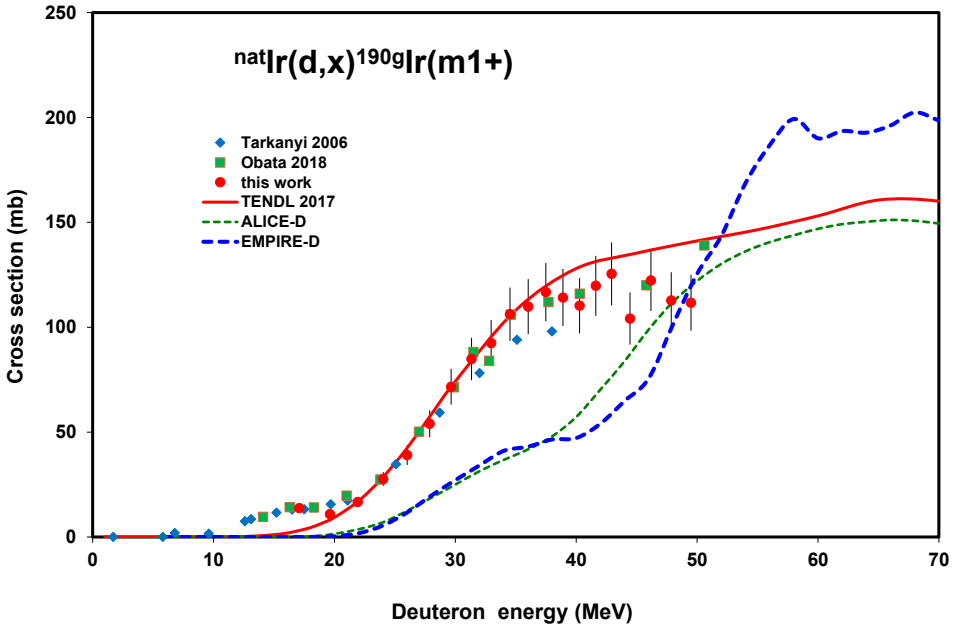

Fig. 11. Excitation function of the ^{nat}Ir(d,x)^{190g}Ir(m1 +) reaction.

4.1.12. ^{nat}Ir(d,x)^{191g}Os(m1 +) process

The production cross section of the longer-lived ^{191g}Os (15.4 d) were deduced from spectra after complete decay of its shorter-lived isomeric state (12.1 h). The experimental data (low cross sections) are very scattered due to low counting statistics. The agreement is better with the TENDL than with the two other codes (Fig. 15).

4.2. Integral yields

The physical [22,23] yields for production of various Pt and Ir radioisotopes on metal Ir target were calculated from the experimental excitation functions. The integral yields of ^{191,189,188}Pt and ^{194g,192,190m2,190g,189,188,187}Ir are shown in Figs. 16 and 17. No measured experimental yields were found in the literature.

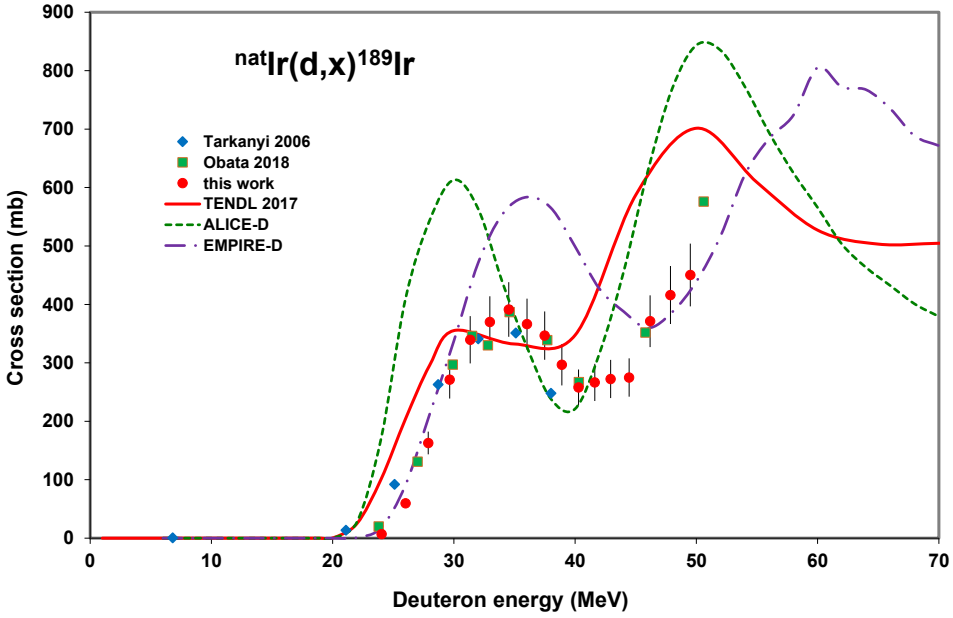

Fig. 12. Excitation function of the ^{nat}Ir(d,x)^{189}Ir reaction.

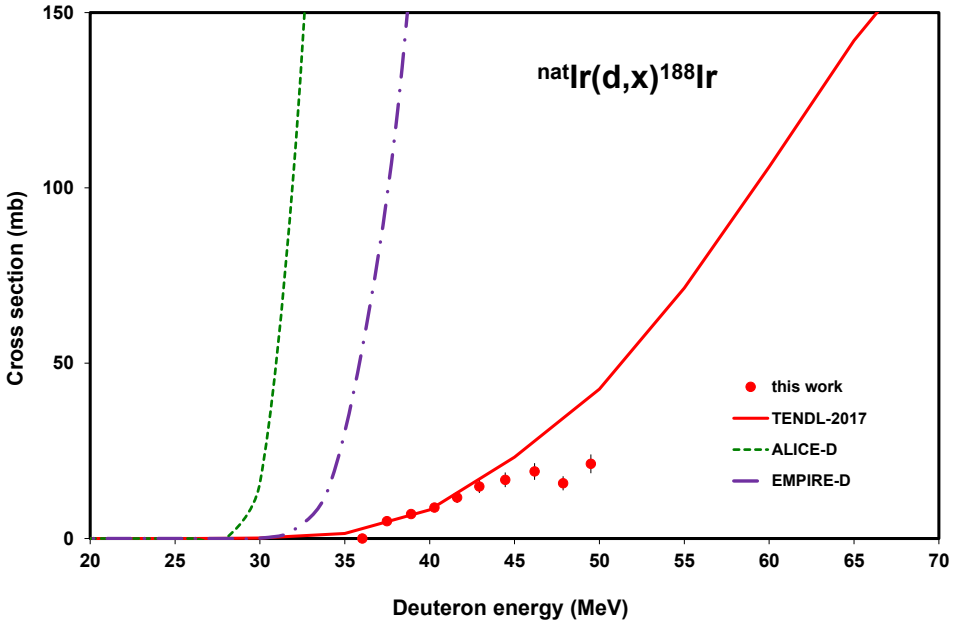

Fig. 13. Excitation function of the ^{nat}Ir(d,x)^{188}Ir reaction.

5. Summary

Activation cross sections of the deuteron induced reactions on iridium were measured for production of ^{193m}Pt, ^{191}Pt, ^{189}Pt, ^{187}Pt, ^{194m2}Ir, ^{194g}Ir(m1 +), ^{192g}Ir(m1 +), ^{190m2}Ir, ^{190g}Ir(m1 +), ^{189}Ir, ^{188}Ir, ^{187}Ir, ^{191g}Os(m1 +) radionuclides in the 17–50 MeV energy range. No earlier data were found for the ^{nat}Ir(d,x)^{187}Pt, ^{190m2,188,187}Ir and ^{191}Os reactions.

The agreement with the earlier experimental data in the overlapping energy range is acceptable. The comparison of the experimental data with the theoretical predictions of ALICE-IPPE-D, EMPIRE-II-D and TALYS codes shows significant disagreement both in shape and in

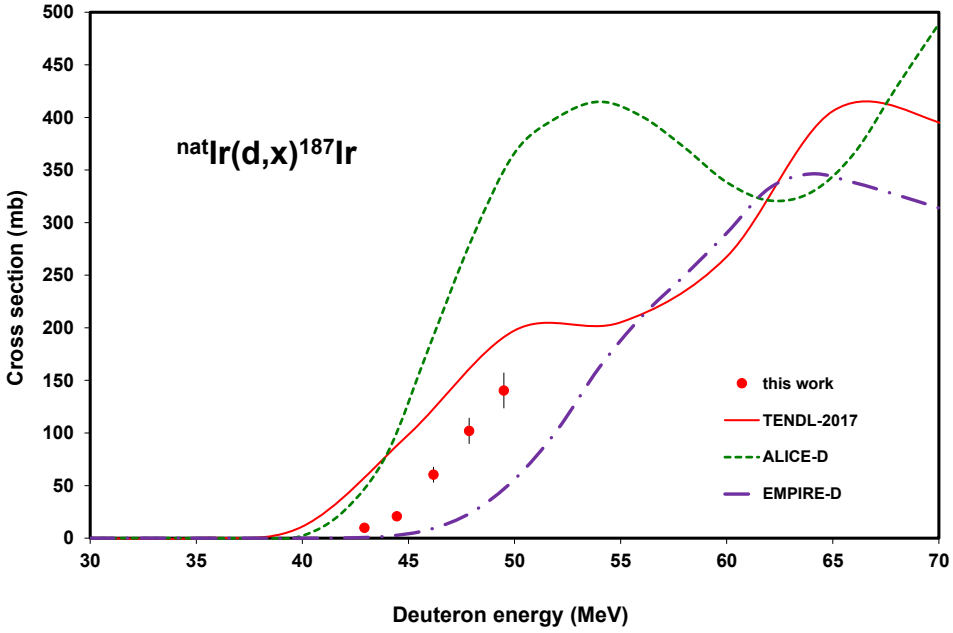

Fig. 14. Excitation function of the ^{nat}Ir(d,x)^{187}Ir reaction.

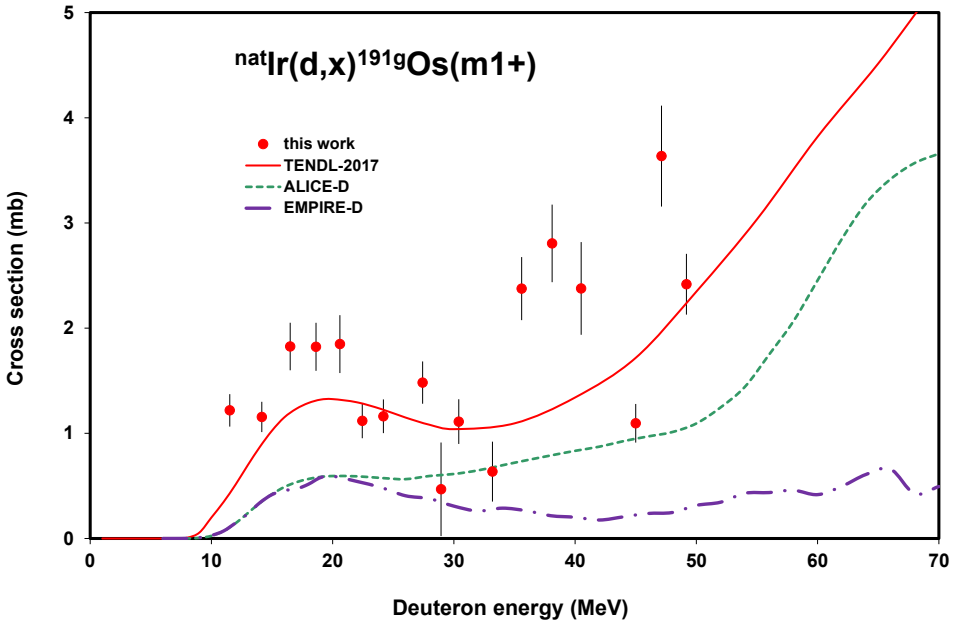

Fig. 15. Excitation function of the ^{nat}Ir(d,x)^{191g}Os(m1 +) reaction.

magnitude, indicating the low predictivity of the codes and importance of experimental data.

The high melting point, hardness and corrosion resistance of iridium and its alloys determine most of its applications among others in nuclear and space industry, where the knowledge the activation data are important. Out of the produced radionuclides the ^{191}Pt (pharmacokinetics of platinum in tumor tissue [24]), ^{193m}Pt (Auger electron emitter, therapy [25]) and ^{192}Ir (brachytherapy source [26]) have medically relevant applications.

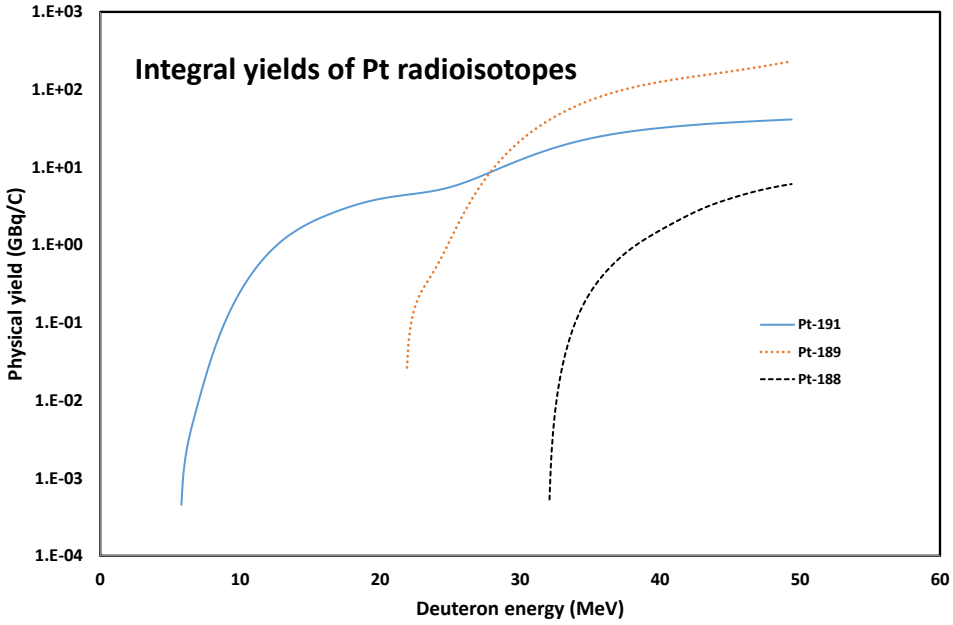

Fig. 16. Calculated Integral yields for production of ^{191,189,188}Pt.

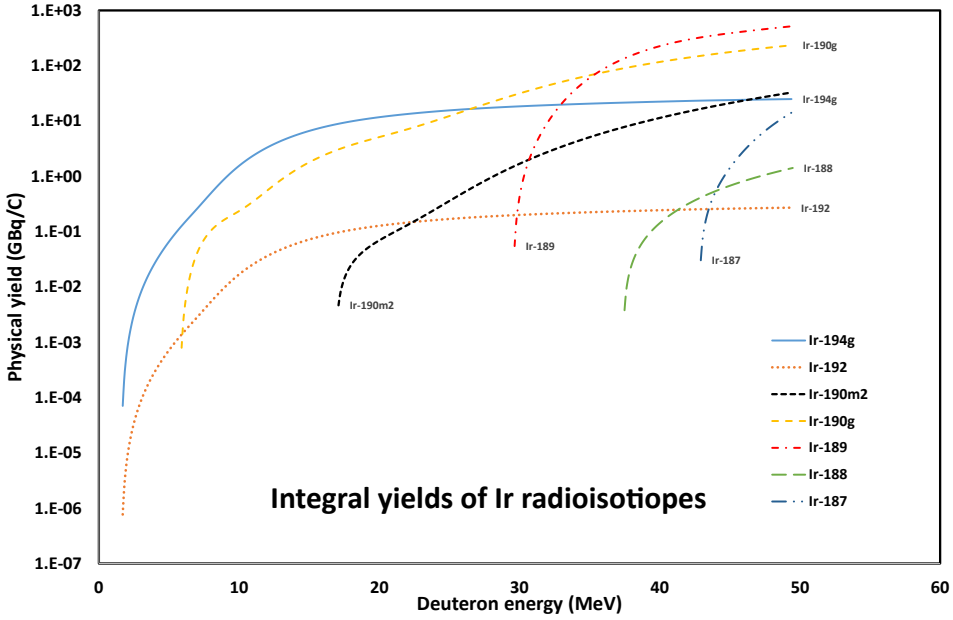

Fig. 17. Calculated Integral yields for production of ^{194g,192,190m2,190g,189,188,187}Ir.

Acknowledgement

The authors of this paper acknowledge the support of the participating institutions and the accelerator staffs for providing the beam time and experimental facilities.

References

[1] F. Tárkányi, A. Hermanne, F. Ditrói, S. Takács, B. Király, G. Csikai, M. Baba, H. Yamazaki, M.S. Uddin, A.V. Ignatyuk, S.M. Qaim, Systematic study of activation cross-sections of deuteron induced reactions used in accelerator applications, in: E. P. Arjan (Ed.) Workshop on Nuclear Measurements, Evaluations and Applications. NEMEA 6, OECD Nuclear Energy Agency, Krakow, Poland, 25-28 Oct., 2010, 2011, pp. 203-214.

[2] F. Tárkányi, B. Király, F. Ditrói, S. Takács, J. Csikai, A. Hermanne, M.S. Uddin, M. Hagiwara, M. Baba, Y.N. Shubin, S.F. Kovalev, Cross sections of deuteron induced nuclear reactions on iridium, Nucl. Instrum. Methods Phys. Res., Sect. B 247 (2006) 210–216.

[3] H. Obata, M.U. Khandaker, E. Furuta, K. Nagatsu, M.R. Zhang, Excitation functions of proton- and deuteron-induced nuclear reactions on natural iridium for the production of Pt-191, Appl. Radiat. Isot. 137 (2018) 250–260.

[4] A.I. Dityuk, A.Y. Konobeyev, V.P. Lunev, Y.N. Shubin, New version of the advanced computer code ALICE-IPPE, in: INDC (CCP)-410, IAEA, Vienna, 1998.

[5] A.J. Koning, D. Rochman, J. Kopecky, J.C. Sublet, E. Bauge, S. Hilaire, P. Romain, B. Morillon, H. Duarte, S. van der Marck, S. Pomp, H. Sjostrand, R. Forrest, H. Henriksson, O. Cabellos, G. S., J. Leppanen, H. Leeb, A. Plompen, R. Mills, TENDL-2015: TALYS-based evaluated nuclear data library, in, https://tendl.web.psi.ch/tendl_2015/tendl2015.html, 2015.

[6] M. Herman, R. Capote, B.V. Carlson, P. Oblozinsky, M. Sin, A. Trkov, H. Wienke, V. Zerkin, EMPIRE: Nuclear reaction model code system for data evaluation, Nucl. Data Sheets 108 (2007) 2655–2715.

[7] A.J. Koning, D. Rochman, J.C. Sublet, TENDL-2017 TALYS-based evaluated nuclear data library, https://tendl.web.psi.ch/tendl_2017/tendl2017.html, 2017.

[8] A. Hermanne, A.V. Ignatyuk, R. Capote, B.V. Carlson, J.W. Engle, M.A. Kellett, T. Kibedi, G. Kim, F.G. Kondev, M. Hussain, O. Lebeda, A. Luca, Y. Nagai, H. Naik, A.L. Nichols, F.M. Nortier, S.V. Suryanarayana, S. Takacs, F.T. Tarkanyi, M. Verpelli, Reference cross sections for charged-particle monitor reactions, Nucl.

Data Sheets 148 (2018) 338–382.
[9] F. Tárkányi, A. Hermanne, F. Ditrói, S. Takács, A.V. Ignatyuk, Activation cross sections of deuteron induced reactions on natHf in the 12–50 MeV energy range, Nucl. Instrum. Methods Phys. Res., Sect. B 441 (2019) 93–101.
[10] G. Székely, Fgm - a flexible gamma-spectrum analysis program for a small computer, Comput. Phys. Commun. 34 (1985) 313–324.
[11] Canberra, http://www.canberra.com/products/radiochemistry_lab/genie-2000-software.asp, 2000.
[12] NuDat, NuDat2 database (2.6), in, National Nuclear Data Center, Brookhaven National Laboratory, 2014.
[13] S.Y.F. Chu, L.P. Ekström, R.B. Firestone, WWW Table of Radioactive Isotopes, version 2.1 http://ie.lbl.gov/toi/, 2004.
[14] B. Pritychenko, A. Sonzogni, Q-value Calculator, NNDC, Brookhaven National Laboratory, 2003.
[15] International-Bureau-of-Weights-and-Measures, Guide to the expression of uncertainty in measurement, 1st ed., International Organization for Standardization, Genève, Switzerland, 1993.
[16] H.H. Andersen, J.F. Ziegler, Hydrogen stopping powers and ranges in all elements. The stopping and ranges of ions in matter vol. 3, Pergamon Press, New York, 1977.
[17] F. Tárkányi, F. Szelecsényi, S. Takács, Determination of effective bombarding energies and fluxes using improved stacked-foil technique, Acta Radiol., Suppl. 376 (1991) 72.
[18] J.F. Ziegler, SRIM-2013 http://www.srim.org/ – SRIM, 2013.
[19] A.V. Ignatyuk, 2nd RCM on FENDL-3, in, IAEA, Vienna, Austria, 2010.
[20] T. Belgya, O. Bersillon, R. Capote, T. Fukahori, G. Zhigang, S. Goriely, M. Herman, A.V. Ignatyuk, S. Kailas, A. Koning, P. Oblozinsky, V. Plujko, P. Young, Handbook for calculations of nuclear reaction data: Reference Input Parameter Library. http://www-nds.iaea.org/RIPL-2/, IAEA, Vienna, 2005.
[21] A.J. Koning, D. Rochman, Modern nuclear data evaluation with the TALYS code system, Nucl. Data Sheets 113 (2012) 2841–3172.
[22] M. Bonardi, The contribution to nuclear data for biomedical radioisotope production from the Milan cyclotron facility, in: K. Okamoto (Ed.) Consultants Meeting on Data Requirements for Medical Radioisotope Production, IAEA, INDC(NDS)-195 (1988), Tokyo, Japan, 1987, pp. 98-112.
[23] N. Otuka, S. Takacs, Definitions of radioisotope thick target yields, Radiochim. Acta 103 (2015) 1–6.
[24] J. Areberg, Studies of radioactive cisplatin (platinum-191) for tumour imaging and therapy, 2000.
[25] F.F.R. Knapp, A. Dash, Radipharmaceuticals for Therapy, Springer, New Delhi, New York, Heidelberg, Dordreeht, London, 2016.
[26] S.R.W. Nurkic, A.I. Ocampo, M.J.P. Gadea, J.C. Greenwalt, M.J. Vicente, A.L. Velasquez, L.C.L. Peralta, F.S. Herrera, O.C. Romero, F.L. Tenorio, H.L. Zamora, L.M. Munguia, A.R. Yeung, The successful implementation of high-dose-rate 192-Ir brachytherapy for cervix cancer in a low-middle income country, Int. J. Radiation Oncol. Biol. Phys. 96 (2016) E292.